Optical Properties of Silver-Coated Silicon Nanowires: Morphological and Plasmonic Excitations

R. M. Abraham Ekeroth & M. Lester

Plasmonics

ISSN 1557-1955

Plasmonics
DOI 10.1007/s11468-013-9555-5

Springer

Plasmonics
DOI 10.1007/s11468-013-9555-5

Optical Properties of Silver-Coated Silicon Nanowires: Morphological and Plasmonic Excitations

R. M. Ekeroth Abraham · M. Lester

Received: 17 December 2012 / Accepted: 8 April 2013

Abstract The optical extinction spectra of micro- and nanoparticles made up of high-contrast dielectrics exhibit a set of very intense peaks due to the excitations of morphology-dependent resonances (MDRs). These kind of resonances are well known at the microscopic scale as whispering gallery modes. In this work, we study numerically the optical spectra corresponding to a core–shell structure composed by an infinite silicon nanowire coated with a silver shell. This structure shows a combination of both excitations: MDRs and the well-known surface plasmon resonances in dielectric metallic core–shell nanoparticles (Ekeroth Abraham and Lester, Plasmon 2012). We compute in an exact form the complete electromagnetic response for both bare and coated silicon nanowires in the range of 24–200 nm of cross-sectional sizes. We take into account an experimental bulk dielectric function of crystalline silicon and silver by using a correction by size of the metal dielectric function. In this paper, we consider small silver shells in the range of 1–10 nm of thickness as coatings. We analyze the optical response in both the far and near fields, involving wavelengths in the extended range of 300–2,400 nm. We show that the MDRs excited at the core are selectively perturbated by the metallic shell through the bonding and antibonding surface plasmons (SPs). This perturbation depends on both the size of the core and the thickness of the shell, and, as a consequence, we get an efficient tuneable and detectable simple system. Our calculations apply perfectly to long nanotubes compared to the wavelength for the two fundamental polarizations (s, p).

Keywords Core–shell nanowires · Plasmonics · Morphology-dependent resonances

Introduction

Optical whispering-gallery modes [2, 3], electromagnetic resonances that can be interpreted by total internal reflection of the light at the surface inside a micro-scatterer, are in fact a kind of morphology-dependent resonances (MDRs), which are showed by micro- and nanoparticles with high relative dielectric constants, like silicon or semiconductor particles in vacuum or in water. From a mathematical point of view, optical MDRs can be found as singularities in the coefficients of Mie series and can be labeled with integer numbers in a similar form to quantum problem of eigenvalues [4]. MDRs, depending of the polarization of the excitation, are more or less confined within the particle showing a huge electric near-field enhancement.

There have been great advances in the synthesis of compounds involving silicon or silica composites with or without plasmonic nanoparticles [5–9], some of them oriented to some particular applications as batteries and photovoltaic cells [10–12], plasmonic applications like waveguiding [13] up to biological tracers [14]. Some applications and studies try to take advantage from other properties, which, in addition, has this kind of semiconductor due the presence of dopants or due the effect of quantum confinement

R. M. Ekeroth Abraham (✉) · M. Lester
Grupo de Óptica de Sólidos-Elfo, Centro de Investigaciones en Física e Ingeniería del Centro de la Provincia de Buenos Aires, Instituto de Física Arroyo Seco, Facultad de Ciencias Exactas, Universidad Nacional del Centro de Provincia de Buenos Aires. Consejo Nacional de Investigaciones Cientficas y Técnicas (CONICET), Pinto 399, CP 7000, Tandil, Buenos Aires, Argentina
e-mail: mabraham@exa.unicen.edu.ar

Published online: 15 May 2013

(particles with sizes less than 5 nm), like luminescence [14–16], fluorescence [17], etc.

In this sense, a great effort has been dedicated to understand the optical properties of systems consisting of bare crystalline silicon structures or composite systems (metamaterials) like silicon metal core–shell systems [18–21]. Many of these systems with high-contrast materials show resonant properties in a wide range of the electromagnetic spectrum. This possibility of tuning these morphological resonant modes, in combination with plasmonic ones, makes these metamaterials very interesting for possible technological applications [22]. In this work, we propose to analyze the linear optical response (through the optical efficiencies Q: absorption, extinction, and scattering, respectively—Q_{abs}, Q_{ext}, and Q_{sca}) of long silicon core–silver shell nanowires (silicon-filled silver nanotubes (nts)), with the aim of characterizing optically such metamaterials (systems). We chose silver as the plasmonic material because it generates sharper resonances than gold or other similar real metals. It makes possible to identify and characterize plasmonic peaks in the extinction or absorption spectra. In particular, the silicon core can have absorption peaks in the range of wavelengths of 600–900 nm, depending on the radius. This optical windows is characteristic of radiation penetration in tissues, and it is considered for biological applications [23, 24].

In the first part of this paper, we review the main optical properties of both plasmonic (hollow) nts and bare silicon nanowires. We derive an analytical expression that realizes evolution of plasmonic resonances with the scaled shell thickness d/r_1, r_1 being the total size of the nt. As we showed in a previous paper [25], for thin metallic shells (in the range of 1–10 nm), it is necessary to correct the dielectric function with d. Next, we briefly review the experimental dielectric function for silicon [26], and we do a complete analysis of MDRs in nanowires constructed with this material.

The second part of the paper is dedicated to a numerical study on the core–shell system. We show that such a kind of combinations between shells of plasmonic materials and silicon cores (or materials with high dielectric constant) allows a tuning of plasmonic modes and MDRs by varying d. For the cases studied in this paper, we found that the plasmonic and morphology-dependent resonances do not interact each other, and the system does not show any coupling resonance.

For our calculations, we use an integral method that solves the Maxwell equations for the imposed geometry of the two fundamental polarizations: s (p) electric (magnetic) field parallel to the cylinder axis. This method does not require any approximation. It is based on the well-known *extinction theorem* and has been used extensively [1, 27, 28]. This method provides some advantages compared, for example, with the calculations by Mie series, in respect to symmetry breaking or calculating the response of other particle shapes. For more details about this method applied to 2D core–shell structures, see the work in http://users.exa.unicen.edu.ar/mlester/764TesisAbraham.pdf (theoretical aspects and numerical implementation). For the silicon core, we use a realistic bulk dielectric function, taking special care in the size of the cores (i.e., for sizes up to 20 nm, the bulk dielectric constant is valid [15, 29–32]). And for the case of small metallic coatings, we use the corrected function showed in [25, 33]. In this way, we can obtain numerically realistic optical spectra for nanowires and nts that are normally illuminated by plane waves.

Plasmonic Properties of the Nanometer Metallic Shells: Metallic Nanotubes

In this section, we review the general optical properties of the nts with thin metallic shells and the dependence of the dielectric function with the shell thickness. The results of this section will be useful in understanding the optical response of core–shell systems with thin shells.

Size Correction of the Dielectric Function

To make a proper description of the electromagnetic interaction with the core–shell system, we use a parametric correction from the complex dielectric function of the bulk material to consider the finite thickness of the metal layer [25]. This correction takes into account the interaction of the conduction electrons with the boundaries of the shell. The complex dielectric function, $\epsilon = \epsilon' + i\epsilon''$, can be decomposed in two additive terms, corresponding to bound and free-electron contributions:

$$\epsilon_{\text{bulk}}(\omega) = \epsilon_{\text{bound}}(\omega) + \left[1 - \frac{\omega_p^2}{\omega^2 + i\omega\gamma_{\text{bulk}}}\right], \tag{1}$$

where ω_p is the bulk plasma frequency and γ_{bulk} is the bulk damping constant. The bound-electron contribution is considered independent of the radius and can be calculated by subtracting the free-electron term from $\epsilon_{\text{bulk}}(\omega)$ [33]. As it is well known from the literature, ω_p is assumed to be independent of the size for particles with radii smaller than the mean free path of conduction electrons in the bulk metal. On the other hand, the damping constant is dominated by collisions with the particle boundary. To take this fact into consideration, it may be written as follows:

$$\gamma_{\text{size}}(d) = \gamma_{\text{bulk}} + C\frac{v_{\text{F}}}{d}, \tag{2}$$

where v_{F} is the electron velocity at the Fermi surface, $d = |r_1 - r_2|$ is the metallic shell thickness of the cylinder, $r_{1(2)}$ are the outer (inner) radius of the structure, and

C is a constant whose value is typically close to unity and depends strongly on the geometry and number of dimensions of the scatterer. The real and the imaginary parts of the free-electron contribution to the dielectric function for a metallic shell of size d can be rewritten as follows:

$$\epsilon'_{\text{size, free}}(\omega, d) = 1 - \frac{\omega_p^2}{\omega^2 + [\gamma_{\text{size}}(d)]^2}; \tag{3}$$

$$\epsilon''_{\text{size, free}}(\omega, d) = \frac{\gamma_{\text{size}}(d)\,\omega_p^2}{(\omega^2 + [\gamma_{\text{size}}(d)]^2)\omega}. \tag{4}$$

The corrected values of $\epsilon'(\omega, d)$ and $\epsilon''(\omega, d)$, which include both free and bound-electron contributions, allow recalculating $\nu_{\text{size}}(\lambda, d)$ and $k_{\text{size}}(\lambda, d)$ (real and imaginary parts of complex metal refractive index, respectively) as a function of thickness. The metal bulk dielectric function used in this work is calculated from experimental values of refraction index ν and k given by Palik [26]($\epsilon' = \nu_2 - k_2$), and $\epsilon'' = 2\nu k$). Values for $\omega_p = 1.38 \times 10^{16} s^{-1}$ and $\gamma_{\text{bulk}} = 2.7 \times 10^{13} s^{-1}$ were taken from Kreibig [34] for silver. The Fermi velocity at room temperature takes the value of 1.39×10^{15} nm/s for Ag.

The complete expression for the complex dielectric function is made up by a free-electron component and a bound electron component:

$$\epsilon(\omega) = \epsilon_{\text{free}} + \epsilon_{\text{bound}} = \epsilon'(\omega) + i\epsilon''(\omega) \tag{5}$$

where ϵ_{free} can be made size-dependent through the Eqs. 3 and 4. In a first approximation, the bound contribution may be considered nonsize- dependent. Its value may be determined from subtracting ϵ_{free} from the bulk experimental data $\epsilon(\omega)$ taken from Palik [26] such as indicated in Eq. 5. For shells with a size smaller than 10 nm, the full complex dielectric function depends on size $\epsilon(\omega, d)$ and can be written as follows:

$$\epsilon(\omega, d) = \epsilon_{\text{free}}(\omega, d) + \epsilon_{\text{bound}}(\omega), \tag{6}$$

where $\epsilon_{\text{free}}(\omega, d)$ of Eq. 6 can be calculated by Eqs. 3 and 4 (for details, see [25]).

In Fig. 1, we show the corrected silver dielectric function for several shell thicknesses as a function of the wavelength λ. The bulk function has been interpolated from the experimental data [26].

Figure 1b shows that the main feature of this dielectric function is the strong increment of the imaginary part (absorption) of the function as the thickness of the shell is decreased. The range of variation for the relative real part (Fig. 1a) is shorter with the thickness. The shift of the values of the curves with the thicknesses implies that, in a fixed value of the real dielectric function, there is a red shift of the corresponding values of the curves that could play a relevant role in a fixed pole of resonance of the system. On the other hand, in the curves from the real and imaginary parts, we see a change in the behavior of the curves at wavelengths near 325–330 nm, these being the effect of the interband transitions in silver (see, for example, [35]).

In the next subsection, we perform a brief description of the plasmonic resonances in nts where the variations of the dielectric function of the metal shell are considered.

Plasmonic Resonances of the Nanotubes

The core–shell structures or nanoshells for 2D and 3D geometries have been extensively studied [36–38]. In general, for metallic shells with a dielectric core, a model for no retardation problems is used, which involves solutions of the Laplace equation (electrostatic approximation) and where the complex Drude dielectric function is considered. This is usually called the *plasmon hybridization model* [39] and concerns an analogy between the plasmonic solutions of core–shell systems and quantum solutions for molecules obtained as superposition or hybridization from wave functions of single atoms. For the 2D case, Moradi [40] predicted the resonances and dispersion curves corresponding to nanotube structures (i.e., metallic shell with an air core) by means of the hybridization model. The equation that was obtained is

$$\omega_{\pm}^2(l, q = 0) = \frac{\omega_p^2}{2}\left[1 \pm \left(\frac{r_2}{r_1}\right)^l\right]. \tag{7}$$

where l is the angular momentum number. This equation in the limit of nonretarded problem seems explicitly independent of d, as a first approximation, and leaves $\frac{\omega_{\pm}^2}{\omega_{\text{sp}}^2} = \left[1 \pm \left(\frac{r_2}{r_1}\right)^l\right]$ if we take the SP limit $\omega_{\text{sp}}^2 = \frac{\omega_p^2}{2}$ (see, for instance, [41]), as follows from the Drude dielectric function.

It is instructive to note that we can obtain the Eq. 7 by another way that Moradi did. We start from the Eq. 10 in the paper [42] for surface resonance modes,

$$\left(\frac{r_2}{r_1}\right)^{2l}(\varepsilon_0 - \varepsilon_1)(\varepsilon_1 - \varepsilon_2) + (\varepsilon_0 + \varepsilon_1)(\varepsilon_1 + \varepsilon_2) = 0, \tag{8}$$

where ε_i $(i = 0, 1, 2)$ corresponds to the embedding/shell/core medium, respectively. This equation arises from considering the poles of Mie coefficients for p mode under the asymptotic approximation of Bessel and Hankel functions (for 2D core–shell structures) for small arguments.

When we consider the Drude model (without losses) in the dielectric function ε_1 for the metal shell and

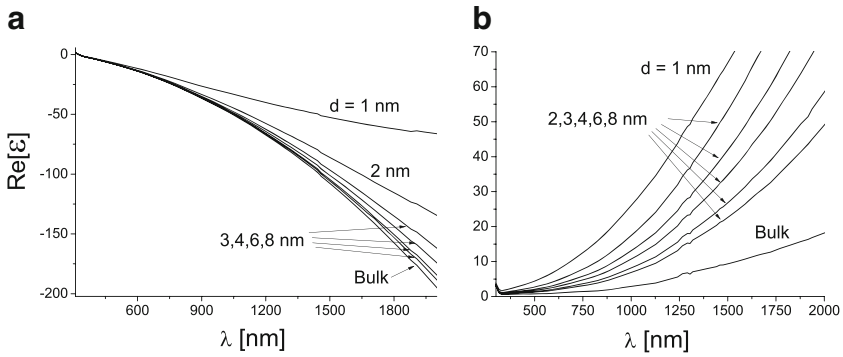

Fig. 1 Bulk and corrected dielectric function by shell thickness d for thin silver shells as a function of the wavelength. **a** Real part. **b** Imaginary part. The different thicknesses d are labeled in the respective panels

$\varepsilon_2 = \varepsilon_0 = 1$ for the rest of relative permittivities, the Eq. 8 gives

$$\left(\frac{r_2}{r_1}\right)^{2l} (1-\varepsilon_1)^2 = (1+\varepsilon_1)^2, \tag{9}$$

$$\left(\frac{r_2}{r_1}\right)^{2l} \left(\frac{\omega_p^2}{\omega^2}\right)^2 = \left(2-\frac{\omega_p^2}{\omega^2}\right)^2,$$

equation that generates the two solutions

$$\pm\left(\frac{r_2}{r_1}\right)^{l} \frac{\omega_p^2}{\omega^2} = \left(2-\frac{\omega_p^2}{\omega^2}\right),$$

extracting the common factor $\frac{\omega_p^2}{\omega^2}$, one obtains

$$\left[1 \pm \left(\frac{r_2}{r_1}\right)^{l}\right] \frac{\omega_p^2}{\omega^2} = 2, \tag{10}$$

which is the Moradi relation (Eq. 7).

We can see that if $r_1 \longrightarrow \infty$, this equation would return the modes excitable in a surface rounding a semi-infinite bulk material, and, as the curvature of the particles tends to zero, the modes consist of those corresponding to flat surface modes. But if $r_2 \longrightarrow 0$, this equation would correspond to the modes of a bare nanoparticle of radius r_1. In this limit, however, Eq. 10 gives again the flat surface plasmon $\omega_{sp} = \frac{\omega_p}{\sqrt{2}}$, a constant value for the same metal. It has been shown in previous works [43] that the frequency or wavelength of excitation of a SP of bare nanoparticle depends on the radius ($r_1 \lesssim 20$ nm). This feature indicates the importance of using a size correction for the metal dielectric function, specially when we observe the optical spectrum for small particles, and it is the main failure of taking the above expression.

We understand that this result is due to the approximations in the used model. The Drude function for the dielectric constant of a metal does not adjust well to experimental values [35] in the range of short wavelengths (UV–visible). This discrepancy is mainly due to the free-electron model used by Drude to describe the behavior of the dielectric constant with the frequency. This model does not take into account the contribution due to bound electrons to the dielectric function or even the losses in the system. Our model incorporate the contributions of the interband transitions and the size dependence of the resonances[25].

The analysis made corresponds to the extreme cases of Eq. 10. For intermediate cases, relationship 10 offers an alternative way of explaining the well-known universal size scaling of the dipolar (i.e., when $l = 1$) optical peaks obtained in the spectra of some plasmonic particles, as the core–shell system or nts (or 3D nanoshells), because the position of peaks of the excitations (the real part of the poles of Mie coefficients) is expected to be not changed so far. At least, it provides another justified approach different from that used in previous works in [44, 45] or in [46], where it is assumed that the scaling laws can be adequately reproduced by exponential curves. If we express 10 as an adimensional scaled equation, as typically have appeared, for example, in ref [44], it follows that

$$\frac{\omega^2}{\omega_{sp}^2} - 1 = \pm\left(\frac{r_2}{r_1}\right)^{l} \rightarrow \frac{\omega^2-\omega_{sp}^2}{\omega_{sp}^2} = \frac{\triangle\omega^2}{\omega_{sp}^2} = \pm(1-\chi)^l,$$

where $\chi = d/r_1 = (r_1 - r_2)/r_1$ is one adequate adimensional parameter that represents the core–shell structure in our present case of geometry. We can follow one of the two expected dipolar resonances (the strongest, since we expect to be able to detect it by far-field measures), then

$$\frac{\triangle\omega^2}{\omega_{sp}^2} = (1-\chi)^l, \tag{11}$$

or equivalently, taking the square root

$$\frac{\triangle\omega}{\omega_{sp}} = (1-\chi)^{l/2}. \tag{12}$$

And taking $l = 1$,

$$\frac{\triangle\omega}{\omega_{\rm sp}} = \sqrt{1-\chi},$$

note that this equation is very different of an exponential behavior.

Unfortunately, as our calculations depend implicitly on the contribution of bound electrons by means of the bulk dielectric function, we cannot arrive at an analytical size scaling law in a way similar to the Eq. 12. In our previous work, we showed that in the limit of bare particles, we could obtain a "real" universal law for dipolar excitations, because the curves reach a common limit independently of the metal material. That kind of scaling was not obtained before, and, in the limit of bare particles, it is due to the electromagnetic similarity [47] that is governed by the conformal symmetry of the Maxwell equations, independently of the dielectric functions used.

Analysis of Shell Resonances

As to illustrate how the resonances evolve in silver shells or hollow nts, we show in Fig. 2 the extinction and absorption spectra (efficiencies) of a shell for several thicknesses. In this case, we fixed the external radius r_1 of the structure. Then the two plasmonic peaks show a dependence with d (see the inset in Fig. 2). As predicted in the Eq. 7 by the hybridization model, two plasmon resonances govern these curves: a resonance at short wavelengths or antibonding and a second one corresponding to long wavelengths or bonding resonance [40, 48]. As the thickness d increases, the bonding and antibonding dipolar resonances of the plasmon tend asymptotically to the unique resonance of a solid particle, with $r = 50$ nm, $\lambda \approx 340$ nm.

As was showed in [25] and previous papers [44, 45], with an adequate normalization of the geometric parameters, it is possible to build a universal curve for plasmonic dipolar resonances in concentric core–shell structures, independently of the radii used.

In Fig. 3, we show a universal curve for Ag nanotube: $\triangle\omega^2/\omega_{\rm sp}^2$. vs $\chi = d/r_1$. In all the cases, solid square points correspond to the maxima of the resonant excitation in extinction cross-sectional curves, computed with the integral method and the size-corrected dielectric function. We verified the dipole nature of these resonances through the calculations of Mie coefficients.

In the same figure, we show two different fits for the computed points. One with the Eq. 11 where l is the adjustment parameter (solid curve) and the other one with an exponential fit as $\triangle\omega^2/\omega_{\rm sp}^2 = Ae^{-bx}$ [44], where A, b are the adjustment parameters in this case (dashed curves). The best values for the fits were found to be $l = 2.21 \pm 0.06$ (which when compared with Eq. 10 is not dipolar), and $A = 1.02 \pm 0.03, b = 3.1 \pm 0.2$. The clear discrepancy in the value of l is due to approximations taken in order to arrive at an analytical formulation like the Moradi expression, Eq. 7. Note that for the exponential fit, it has one more adjustment parameter than the other fit.

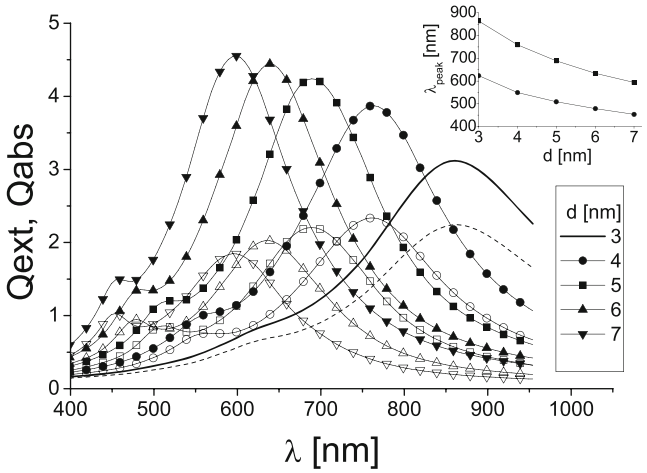

Fig. 2 Optical efficiencies for Ag nts of external fixed radius at 50 nm for various shell thicknesses. *Solid line* and *solid symbols*, the extinction efficiency; *dashed line* and *hollow symbols*, the absorption one. The *inset* shows the evolution of the resonant absorption peaks as d increases. All the cases involve the calculations with the size-corrected dielectric function

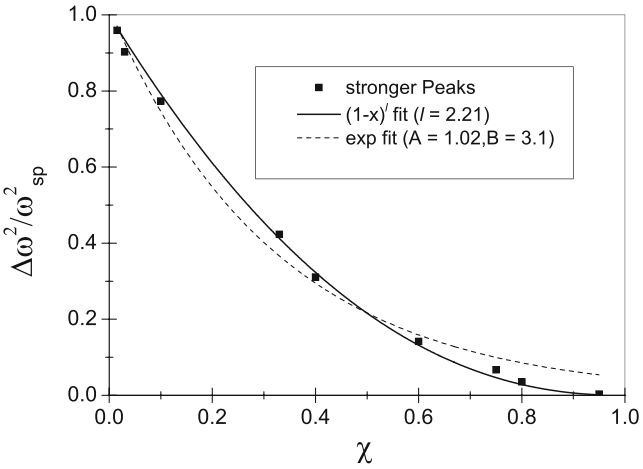

Fig. 3 Scaled dipolar resonances for silver nts. The *solid squares* correspond to the peaks from the spectra calculated by dielectric function with the size correction. The *solid curve* represents the fit for comparing with the hybridization model. The *dashed curve* represents the points computed in Fig. 2. The agreement between the integral method and Mie's expansion is less than 0.01 %, within the numerical error exponential decaying fit. The best values for the fits was found to be $l = 2.21 \pm 0.06$ and $A = 1.02 \pm 0.03$, $b = 3.1 \pm 0.2$

General Optical Properties of Silicon

In this section, we review some optical properties of the bulk silicon and what is expected for Si 2D nps. We begin with a brief discussion about the dielectric function related with the electronic band structure of pure silicon, and next, we analyze the excitation of MDR.

Silicon Constitutive Parameters

In the ref. [49], it is possible to find a complete description of the shape of the bulk silicon band structures. From ref. [49], the silicon has two possible interband transitions. One of them occurs at 1.1 eV (approx. 1,000–1,100 nm) which corresponds to an indirect transition. The second one is a direct transition and occurs at about 3.3 eV (375 nm). This feature is shown in Fig. 4, where we show the behavior of both the real part and imaginary part of the complex dielectric function with the wavelength at 25 °C [50].

The complex dielectric function shows a huge increment in both real and imaginary parts for direct transitions from the valence band (interband transition) near to 375 nm. The lower peak at about 1,000 nm (IR) is the provided by the phonon-assisted transitions inside the silicon. Note that, in the limit of long wavelengths, the imaginary part goes to zero and the real part converges to the well-known dielectric constant of silicon used frequently in the electrostatic approximation [20].

The MDRs of the 2D Silicon nps

From a physical point of view, the MDRs can be understood through a simple model [4, 51]: the corresponding Helmholtz's equation is compared with a Schödinger equation for photons. Using the fundamental modes of polarization of the modes of the problem, one can define "photonic" wave functions (one for each polarization) and make this analogy, inserting adequately the boundary conditions. Differently from the quantum problem, the electromagnetic problem possesses an effective potential that changes as the incident wavelength (plane electromagnetic polarized wave) varies. This is because, in the electromagnetic problem, the energies depend on the adimensional parameter $k_0 a = \frac{2\pi}{\lambda} a$. In this way, the resonances may be identified with semi-stationary states (stationary states that lose their energy by Joule effect, i.e., the refractive index is a complex function and by tunnel effect). In the same manner to the quantum problem, the quasiparticle obtained by the analogy may eventually tunnel the barrier and scatter light [4].

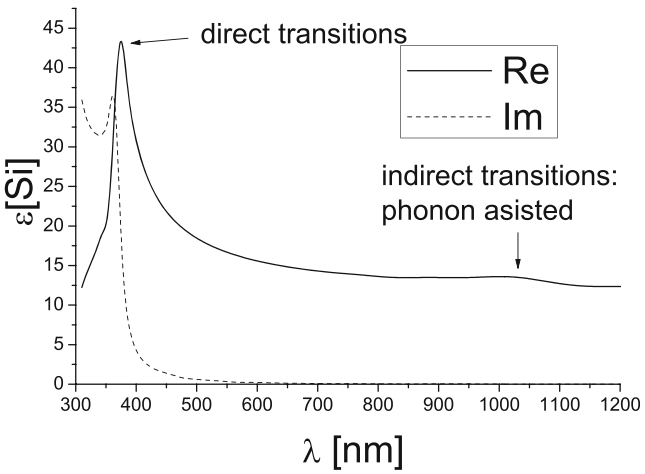

Fig. 4 Bulk silicon dielectric function, interpolation from experimental values at 25 °C. The *solid curve* represents the real part, and the *dashed curve*, the imaginary part. The electronic transitions are labeled

Thus, depending on the relative dielectric function $\varepsilon(r)$ of the particle (and supposing $\mu(r) = 1$), we can obtain a potential well for one photonic wave function that can be scaled to the incident energy, giving quasi-bounding states. We only can obtain appreciable bound states if the dielectric function of the particle is high enough, neglecting the possibility of tunneling (since it is the difference with the centrifugal term in the effective potential that matters [4]). It is interesting to note that this model is independent of the polarization of the electromagnetic waves. The difference with true bound quantum states is that, in the electromagnetic case, the internal losses caused by using complex refractive indexes have to be sustained by the energy of the incident wave. The complete analogy is found when using lossless media.

Due to the fact that general solutions of the Helmholtz equation for particles could be expressed by expansions of Mie, these series allow identifying the contribution of particular multipolar orders in resonant excitations. The optical resonances are related with complex poles in the amplitudes of the multipole scattering functions. Then, in the same manner as a quantum mechanical problem, these electromagnetic resonances can be identified by a set of integral numbers [4]. In a 3D problem, two angular momentum l, m numbers arise. But fixing these l, m, we could find several poles for each denominator of the series, depending of the $k_{\text{eff}} a$ adimensional parameter (where $k_{\text{eff}} = \frac{2\pi}{\lambda}\sqrt{\varepsilon_2 \mu_2}$ is the effective wave number in the particle and a the radii of the particle). If again we fix another parameter as a, the poles that appear are radial modes. These could be called as n_r. For the 2D case, the number m can be ignored since the problem has a one ignorable coordinate (say, for instance, the z coordinate), and we only retain the n_r, l numbers for the scattering of a dielectric circular cylinder.

MDRs' Characterization

With the aim to characterize the evolution of the modes corresponding to MDRs in the range of 10 to 100 nm of radius, we have calculated some optical responses (efficiencies) for silicon nps. In Fig. 5 we show the evolution of the peaks corresponding to resonances of the absorption or scattering efficiency (λ_{peaks}) with the radius for the two fundamental polarizations s and p. The curves of optical efficiencies were computed from the integral method, and the labels (n_r, l) for each resonant peak were obtained from the calculations of the Mie coefficients (we only compute up to the $l = 3$ orders).

For the points computed in Fig. [5], the agreement between the integral method and Mike's expansion is less than 0.01 %, within the numerical error.

At the right of each curve, we indicate the labels (n_r, l). The solid (open) symbols correspond to the s (p) polarization. For the sake of clarity, in the inset panel, we show the order of the next modes that appear at short wavelengths and major radii.

In Fig. 5, we can see how the multipolar terms are entering in the scene, without crossing themselves, at short wavelengths while the radius increases. On the other hand, in the limit of small radius, the different multipolar orders disappear, and the curves seem to converge each other, and for very small particles, i.e., for a 10-nm radius, the s mode optical peaks remain relatively strong (because the $l = 0$ pole survives). The strong resonances in the limit of small sizes can only be seen at high-contrast dielectric particles like silicon or semiconductor nps. It is worth mentioning that the $l = 0$ order is only possible to excite in cylindrical geometry; for 3D geometry, the lowest order is $l = 1$ [52].

It is interesting to note that the s and p curves for resonant peaks are, in general, coincident in n_r, but with a different number l, that is $l_p = l_s - 1$ for p mode (note that $l_{s\,(p)} = 0, 1, 2, 3, ..;$ where $l_{s\,(p)}$corresponds to s (p) polarization), i.e., the p mode "follows" the s mode.

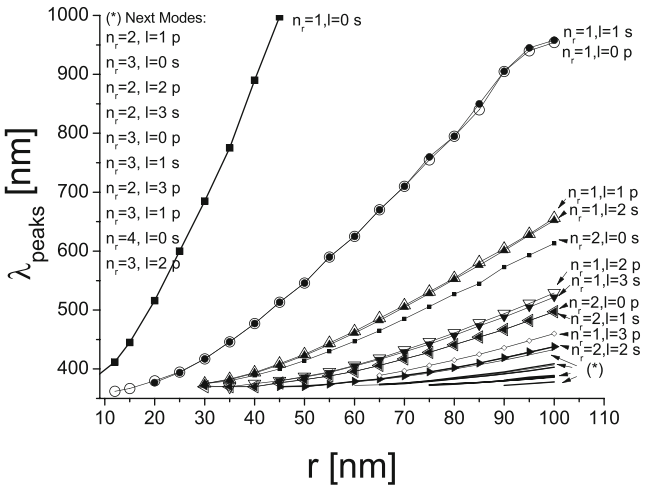

Fig. 5 Evolution of the modes in a silicon nanowire for increasing radius

With the aim of showing the relative intensity of the excitations and the rule $l_p = l_s - 1$, we consider in Fig. 6 two characteristic spectra of both scattering (solid lines) and absorption (dashed lines) efficiencies for silicon nanowires at 50 nm of radius: the panels a and b correspond to s (p) polarization. For each polarization, we identify the peaks of MDRs, and the relationship between $l_s = 0$ and $l_p = 1$ for $n_r = 1$ is clear . The inserted near-field images correspond to the intensity distribution at wavelengths of the excitations. In all these cases, the incident wave impinges from the right at $y = 0$. We can see clearly from the maps of relative intensity that, for p polarization, it reaches up to one order of magnitude greater than the s polarization (see the scales at the right of the images), and the field is strongly confined inside the section of the wire for the p mode, while for the s mode, the intensity distribution spreads out through the contour.

It is interesting to note that, in the neighborhood of 400 nm, near to the direct transitions ($\lambda = 375$ nm for bulk silicon), the efficiency of absorption shows a peak, while the scattering efficiency shows a minimum for the s mode of polarization. This peculiar behavior of the optical response resembles the dark plasmonic modes in metallic nps [53–55]. We have not observed this behavior for p polarization. One possible explanation of this fact could be that the MDRs are overlapping in the range and masking this phenomenon, resulting the absorption and scattering peaks to be shifted in wavelength (see panel b).

Another important feature seen in this figure is that absorption spectrum for s polarization does not contain any information about the first MDR. There is no monopolar absorption by the material because this multipolar contribution cannot prove any internal transition.

Silver–Silicon Structures

In this section, we show the numerical results for the optical response of silicon core–silver shell systems for p polarization where plasmons are excited. We obtain and analyze hybridized spectra formed by the excitation of MDRs and SP resonances.

Optical Response of Small Core–Shell Structures ($r_2 = 12$ nm)

We base our analysis on the results shown in the Analysis of Shell Resonances and MDRs' Characterization

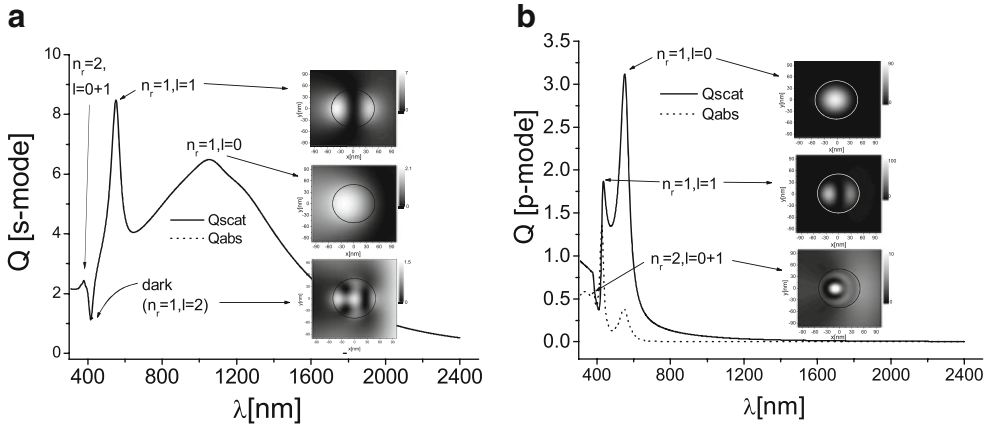

Fig. 6 **a**, **b** Scattering (*continuous line*) and absorption (*dashed line*) efficiencies for a silicon nanowire of the radius of 50 nm and identification of the MDRs. Panels **a** and **b**, for s (p) polarization. *Inset* **a**: Relative intensity distributions in the near field around the wires at the s resonances in the spectrum shown in **a**. For the mode $(n_r = 1, l = 0)$ at 1,550 nm, for $(n_r = 1, l = 1)$ at 550 nm, for $(n_r = 1, l = 2)$ at 421 nm; *inset* **b**: relative intensity distributions in the near field around the wires at the p resonances shown in **b**. For $(n_r = 1, l = 0)$ at 550 nm, for $(n_r = 1, l = 1)$ at 430 nm, and for mixed mode $(n_r = 2, l = 0 + 1)$ corresponding to the scattering peak at 378 nm

sections. The new hybrid system shows a set of modified MDRs originated in the silicon core bounded by plasmonic shell excitations. We begin to study small nps where the optical response is dominated by the absorption, and in Fig. 5, we expect only a MDR corresponding to dipolar excitations.

Figure 7 shows the absorption spectra for a core $r_2 = 12$ nm with a silver shell of variable thickness for p polarization. We vary the thicknesses from $d = 0$ (solid line) to 10 nm (open triangles). The $d = 0$ curve corresponds to the absorption spectrum of the bare silicon nanowire. We indicate the SP resonances and the first MDR weakly excited

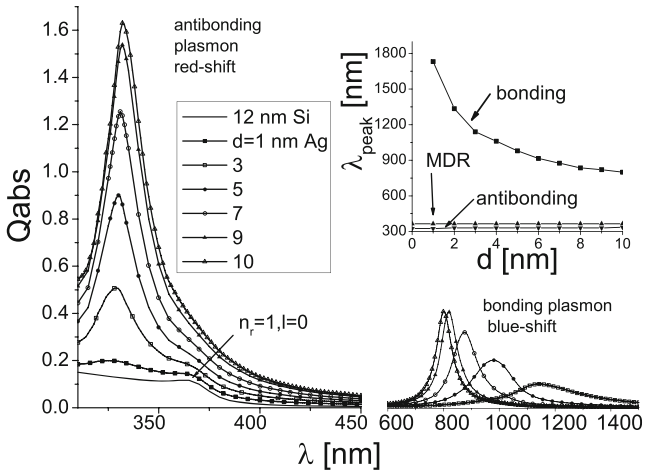

Fig. 7 Absorption spectra of Si core $r_2 = 12$ nm Ag shell systems of several metallic shell thicknesses for p polarization. The *inset* shows the dispersion behavior of the peaks at wavelength λ_{peak} for different d. The silicon MDR and the two plasmonic resonances are indicated in the *inset*

$(n_r = 1, l = 0)$. This MDR is practically undetectable even for thin shells due to the enhancement of the bonding and antibonding SP resonances when the metallic shell d increases. In another way, the bonding SP resonances are strongly blueshifted, and it makes this structure tuneable (see the inset). In the inset (λ_{peak} vs. d), we show the dispersion of the peaks as d increases. The curve corresponding to the bonding plasmon shows clearly the blueshift, while the MDR and antibonding plasmon curves are almost constant. This behavior is due mainly to the interband transitions [25] taken into account in the dielectric function of silver, Eqs. 3 and 4. In this case, $r_2 = 12$ nm of core radius, the "core mode" is not modified (almost static in frequency) when d is increased.

To visualize the behavior of the both plasmonic resonances and MDRs of these nps, we compute the near-field intensity distributions $|H_z/H_{z0}|^2$ (Fig. 8) (the different examples were chosen for a better visualization of the resonant effects). Figure 8a shows the intensity distribution for a bonding plasmon resonance at $\lambda = 875$ nm and $d = 7$ nm; in Fig. 8b, antibonding plasmon resonance for $d = 10$ nm and $\lambda = 330$ nm; and in Fig. 8c, MDR when $d = 1$ nm and $\lambda = 365$ nm. In all cases, the incidence is from the right, at $y = 0$. The resonance shown in panel a is strongly localized in dielectric core–metal interface ("cavity-like" SP), whereas the resonance shown in the panel b is strongly localized in the dielectric host–metal interface ("wire-like" SP). We observe this behavior even for higher shell thickness d. The first MDR $(n = 1, l = 0)$ excited at the silicon core, is practically unaltered by the metal shell. The amplitude decreases only by 6 % in respect to the bare silicon analog case. The position of the resonances in wavelength is practically the same (variation 0.5 %).

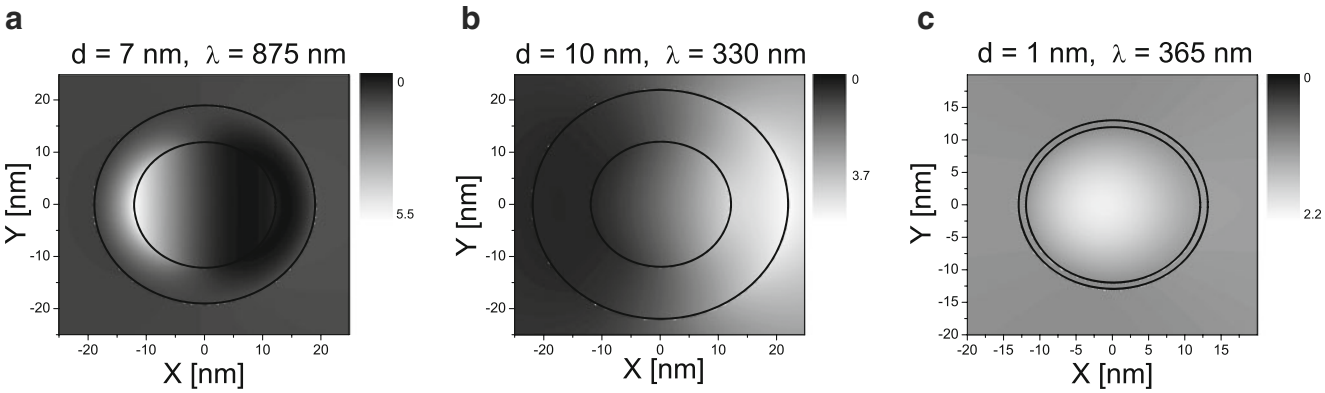

Fig. 8 Relative intensity distribution in the near field around the coated nanowire of Fig. 7 for some characteristic pairs λ, d. The contour of the cylinders of the structure are highlighted for better observation

Intermediate Core–Shell Structures ($r_2 = 50$ nm)

For the next example, we consider a core with 50 nm of radii and variable d thickness. In Fig. 9, we show the evolution of both Q_{ext} and Q_{abs} with the shell thickness for a silicon core of $r_2 = 50$ nm. In the inset, we show the optical efficiencies for the zone of bonding plasmons for this structure. In all cases, the corrected dielectric function is used for calculations, except for the case $d = 10$ nm, where we use the bulk dielectric function for comparison. If we compare Fig. 9 with Fig. 6, we can identify the set of MDRs associated to a bare core.

In this example, the Q_{sca} is not negligible. The main feature for this variation is again the strong shift of the bonding plasmonic mode. If we compare qualitatively the absorption curve with open circles, Fig. 9, with the dashed absorption curve corresponding to Fig. 2 for hollow nts, we can note that the relative intensities between bonding and antibonding resonances have switched: the bonding resonances are damped in intensity, and they are strongly shifted to the far IR zone, whereas the antibonding resonances are strongly blueshifted.

At the chosen range of the parameter d, we observe a small blueshift for the first excited MDR of silicon in respect to the bare silicon nps (that consists mostly in the $n_r = 1, l = 0$ MDR). For this mode, the relative intensity of the peaks remains almost constant in absorption, and it goes diminishing for the Q_{sca} (or Q_{ext}) as d increases. The next excited mode ($n_r = 1, l = 1$ MDR) also presents a small blueshift and small decreasing extinction intensity. The maximum of the scattering spectra occurs for the mode $n_r = 1, l = 0$ for a bare silicon particle (solid curve). This excitation is really a combination of the $l = 0$ and $l = 1$ modes (for $n_r = 1$). For these sizes, there appears another

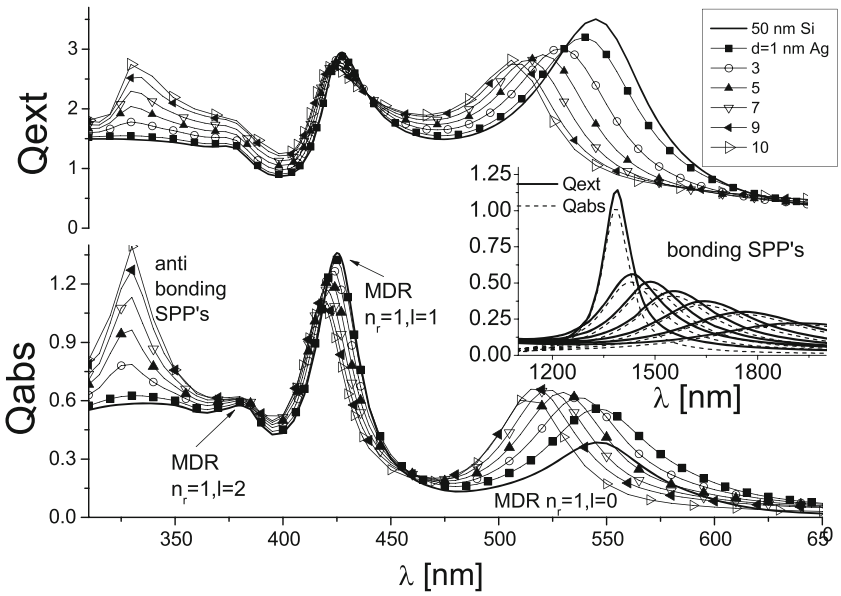

Fig. 9 Optical efficiencies of Si core ($r_2 = 50$ nm) Ag shell systems vs. the incident wavelength for several small shell thicknesses and optical wavelengths. The *solid line* represents a bare core of 50 nm of the radius. The *symbols* represent increasing shells. In the *inset* graphic, the same spectra continue to the far infrared zone. The *solid lines* represent the extinction efficiency; *dashed lines*, the absorption one: these decreasing curves represent $d = 10, 9, 8, 7, 6, 5,$ and 4 nm, respectively. For all the cases except $d = 10$ nm, we use the size-corrected dielectric function where we use the bulk function for comparison

mode, i.e., the $n_r = 1, l = 2$, but it is almost undetectable due the overlapping of the plasmonic antibonding with the peaks $l = 1$ of MDRs.

In Fig. 10, we show the near-field intensity for four interesting wavelengths: panel a, bonding SP resonance; b, $n_r = 1, l = 0$ MDR; c, $n_r = 1, l = 2$ MDR; and d, the antibonding SP resonance. The intensity map for the $n_r = 1, l = 1$ excitation is qualitatively similar to that shown in the inset of Fig. 6b. In all cases, we choose the thickness d according to the best visualization of the resonances.

The bonding plasmon excitation (that is dipolar in nature, i.e., $l = 1$) is visible in the panel a of Fig. 10. This intensity map corresponds to $d = 7$ nm and $\lambda = 1{,}550$ nm (open down-pointing triangles in Fig. 9), where a cavity-like plasmon resonance is appreciated. The near-field enhancement occurs at the Si–Ag interface.

In panel b of Fig. 10, the first MDR is very well detected for a small coating of $d = 1$ nm for $\lambda = 545$ nm. The thin metal layer has a strong absorption for this optical range; therefore, the resonance $l = 0$ is affected by the shell. We can see a decrease in amplitude (17 %) and a slight blueshift (1 %) in respect to the analog resonances of the bare core. The near-field intensification is enclosed inside the core of Si, reaching a maximum value comparable to the bare nanowire. A similar phenomenon occurs at the near-field resonance for the $n_r = 1, l = 1$ mode: the distribution is the same as in the bare core for this mode but presents a small decrease in amplitude (10 %) and a slight blueshift (~ 2 %) due to the presence of the metal shell, in accordance with those showed in Fig. 9 for the far field.

The next mode showed, panel c, is a multipolar mode corresponding to the far-field peak, positioned at $\lambda = 381$ nm for $d = 6$ nm. For this thickness of the shell (not showed in Fig. 9 but similar to $d = 7$ nm, for instance), the resonance of antibonding plasmon shows a broad peak, whose tail overlaps the $n_r = 1, l = 2$ mode, and the same occurs with the $n_r = 1, l = 1$ mode. The intensity map then shows this overlapping of three resonances: three lobes of intensity in the core mainly due to the MDR ($n_r = 1, l = 1+2$) combined with a field intensification on the shell, characteristic of the plasmon resonance.

The last panel shows the intensity map corresponding to the antibonding SP excitation for $d = 7$ nm and $\lambda = 330$ nm. Again, a surface excitation is visible, but it is mainly confined at the air–Ag interface instead at the inner surface.

Moderate Core–Shell Structures ($r_2 = 100$ nm)

A last interesting example to analyze is a core–shell system with a silicon core of $r_2 = 100$ nm of radius. In Fig. 11, we show the Q_{abs} and Q_{ext} efficiencies for different d in the UV–visible (panel a) and visible-IR (panel b) zones of the spectrum. Note in panel a that several MDRs appear, with $n_r > 1$, in addition to the plasmonic resonance. From the absorption spectrum, we can identify seven MDRs due to

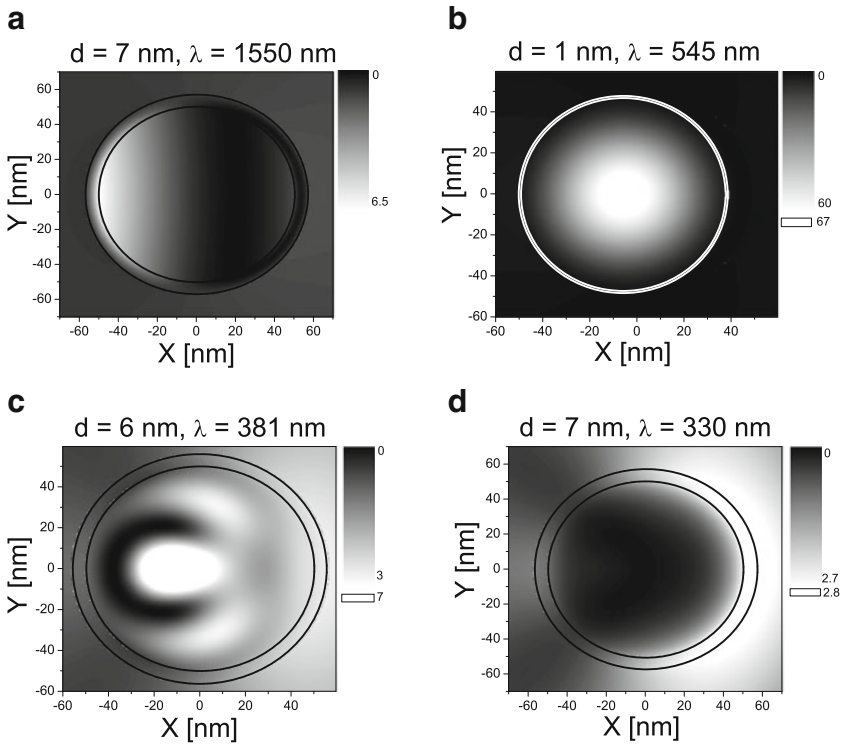

Fig. 10 Near-field images for the resonances that appear in the spectra of Fig. 9. The contour of the cylinders of the structure are highlighted in black or white for better observation. The separate *white color in gray scales* indicate the maximum value reached by the fields (saturation)

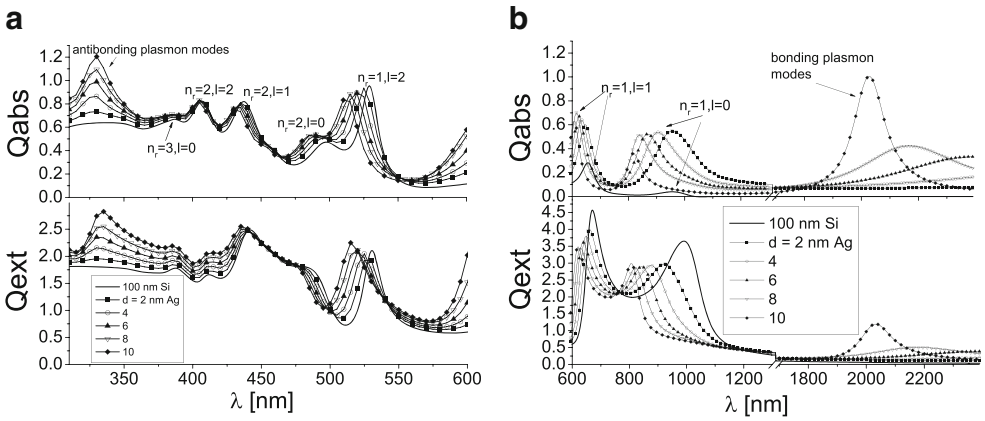

Fig. 11 Optical efficiencies for Si core ($r_2 = 100$ nm) Ag shell systems of small metallic shells with varying d. **a** Short wavelengths and **b** long wavelengths reaching the far-infrared zone

the core and both bonding and antibonding SP modes. As in the previous examples, antibonding plasmon peaks (in all cases) are superposed to the natural Si absorption curve, but the bonding plasmon mode shows a strong absorption peak without any influence of the Si absorption. Note in Fig. 11b that the bonding plasmon peaks for both the absorption and extinction are qualitatively similar in intensity. The scattering is negligible for these low-energy resonances as it is observed in the example of the coated silicon of 50 nm of radius (see inset in Fig. 9).

In contrast to the previous examples, the absorption spectrum of the MDRs are strongly modified by the presence of the metallic shell. The first two peaks of lower orders ($n_r = 1, l = 0$ and $l = 1$) are strongly perturbed by the presence of the shell (compared with the MDRs for bare silicon, solid line). The amplitude of resonances are strongly blue shifted and intensified.

The main difference with previous examples is in the higher-order peaks. Now, the orders $n_r = 1, l = 2$ and $n_r = 2, l = 1$ also exhibit this blueshift, but it is not so marked; these modes are slightly perturbed. The whole spectrum seems "compressed" as the bonding plasmon is blueshifted, while the antibonding mode is almost fixed.

The behavior observed for absorption in amplitude is modified by scattering efficiencies in the extinction curves: the peaks $l = 0$ and $l = 1$ decrease rapidly in amplitude when the thickness of the metallic shell is increased. The scattering governs the extinction curves.

Summary

In this paper, we show results that illustrate the behavior of long silicon nanowires (or 2D silicon particles) coated with a small silver shell. For this purpose, we use a realistic integral method with a size-dependent dielectric function for p mode of polarization. For s mode, no size correction is needed. Our results were supported by a multipolar analysis through calculations of the Mie series, that is, we could identify the multipolar terms in the spectra in an exact form.

As a brief review, we present a study for silicon particles for both polarizations without any coating, and we analyze the MDRs for different radii. We compare both bare silicon nanowires and core–shell systems when the incident plane wave is p polarized. We found in all the examples studied that there is a direct relation between the absorption (or extinction) spectra between both systems: a set of peaks in absorption are identified with MDRs excited in the silicon core, bounded by the bonding and antibonding SPs excited in the metallic shell. For a fixed core radius, the MDRs ses mode ems to be "pushed" to short wavelengths by the bonding plasmon when the thickness shell is increased. The MDRs identified with $l = 0, 1$ and $n_r = 1, 2$ are the most affected by the blueshift effect.

For the sake of brevity, we do not show results for the s mode of polarization for the core–shell system in the Silver–Silicon Structures section. We found in the corresponding absorption spectra that the MDRs are excited at the same wavelengths as those from the case of p mode of incidence and have intensities of the same order, without exciting the SPs which are forbidden for this mode. This is an important feature for applications that are based in the distinguishability of the polarizations.

We can make an interpretation of our numerical results within the framework of Johnson's model [4]. The MDRs can be thought of as resonances of quasi-bound states in an asymmetric potential well, governed by a centrifugal term and a scattering term. The latter functionally depends on the relative dielectric function, through the wave number and size of the particle. The adding of a metallic shell to a silicon nanowire increments the potential barrier to the well, which substantially modifies quasi-bound levels of photonic waves (see, for instance, Fig. 4 of the paper [4]). Whereupon, like the quantum states, the lowest energy states are

more sensible to the relative depth of the well. When the effective potential is modified by the presence of the metallic shell, the silicon MDRs are then modified, decreasing its tunneling probability, leading to a higher confinement of the resonant mode and increasing his relative energy (blueshift). In that way, the lower multipolar terms (i.e., the monopolar and dipolar contributions) are those who play an essential role in the electromagnetic response of these systems.

The response of the core–shell structure can be compared to the response of a "special" dimer through the framework of the plasmon hybridization model [44], where the resonances in spectra arise from the SPs' interactions between a cavity and a solid particle. These corresponds to "shell" resonances. The influence of the dielectric core affects the position and intensity of the resonances from the metallic shell, without involving another interaction peak between the shell and the core, at least in the linear regime (for the importance of nonlinear response, see, for instance, the work in [56], for a dimer composed by a silicon and a silver particle). That phenomenon is due to the different nature of the excitations in the metal shell and in the dielectric core and provides a rich spectra of well-resolved peaks in an extended electromagnetic range, easily tuneable through an adequate design of the structure. This could be exploited for technological applications as biological tracers, by instance, using nanowires or nanoparticles that offer an alternative to use the small nanoparticles in the range of quantum confinement, which optical properties are based in the phenomenon of luminescence.

References

1. Ekeroth Abraham RM, Lester MF (2012) Plasmonics (7):579–587
2. Matsko AB, Ilchenko VS (2006) IEEE J Sel Top Q Elect 12(1):3–14
3. Gorodetsky ML, Fomin AE (2006) IEEE J Sel Top Q Elect 12(1):33–39
4. Johnson BR (1993) J Opt Soc Am A 10:343–352
5. Niitsoo O, Couzis A (2011) J Coll Interf Sci 354:887–890
6. Tang S et al (2007) J Sol Stat Chem 180:2871–2876
7. Amoruso S, Ausanio G et al (2004) App Phys Lett 84(22):4502–4504
8. Zhu SL et al (2011) Surf Coat Tech 205:2985–2988
9. Fojtik A et al (1993) Phys Chem 97:1493–1496
10. Chen H et al (2011) J Pow Sources 196:6657–6662
11. Hu L, Chen G (2007) Nano Lett 7(11):3249–3252
12. Mohapatra S et al (2008) App Phys Lett 92(103105):1–3
13. Krasavin AV, Zayats AV (2010) Opt Exp 18(11):11791–11799
14. O'Farrell N, Houlton A, Horrocks BR (2006) Inter J Nanomed 1(4):451–472
15. Meier C, Wiggers H et al (2007) J App Phys 101(103112):1–8
16. Lin N et al (2011) J Phys Chem C 115:3198–3202
17. Zhuo S-J et al (2010) J App Phys 108(034305):1–4
18. Bardhan R et al (2010) AC Nano 4(10):6169–6179
19. Idrobo JC (2009) Phys Rev B 79(125322):1–6
20. Miroshnichenko AE (2010) Phys Rev A 81(053818):1–5
21. Evlyukhin AB et al (2010) Phys Rev B 82(045404):1–12
22. Kumar V (2007) Nanosilicon. Elsevier, Amsterdam
23. Wang LV, Wu H-I (2007) Biomedical optics: principles and imaging. Wiley, Hoboken
24. Xu C et al (1996) Proc Natl Acad Sci USA (Biophysics) 93:10763–10768
25. Ekeroth RMA, Lester M, Scaffardi LB, Schinca DC (2011) Plasm 6(3):435–444
26. Palik ED (1998) Handbook of optical constants of solids II. Elsevier, Amsterdam
27. Lester MF, Skigin DC (2007) J Opt A: Pure Appl Opt 9:81–87
28. Shu WX, Ren Z, Luo HL, Li F (2007) Eur Phys J D 41:541–546
29. Ma DDD et al (2011) Science 299:1874–1877
30. Tsu R (1997) J App Phys 82(3):1327–1329
31. Ren SY et al (1992) Phys Rev B 45(12):6492–6496
32. van Buuren T et al (1998) Phys Rev Lett 80(17):3803–3806
33. Schinca DC et al (2009) J Phys D Appl Phys 42(215102):1–9
34. Kreibig U (1974) J Phys F Metal Phys 4:999–1014
35. Novotny L, Hecht B (2006) Principles of nano-optics. Cambridge University Press, Cambridge
36. Wu D, Xu XD, Liu XJ (2008) Sol State Comm 146:7–11
37. Prodan E, Nordlander P (2002) Chem Phys Lett 352:140
38. Liu WF, Oh JI, Shen WZ (2011) Nanotechnology 22:125705
39. Prodan E, Nordlander P (2004) J Chem Phys 120(11):5444–5454
40. Moradi A (2008) J Phys Chem Sol 69:2936–2938
41. Maier SA (2007) Plasmonics: fundamentals and applications. Springer, New York
42. She H-Y, Li L-W, Martin OJF, Mosig JR (2008) Opt Lett 16(2):1007–1019
43. Scaffardi LB, Lester M, Skigin D, Tocho JO (2007) Nanotech 18(315402):1–8
44. Jain PK, El-Sayed MA (2007) Nano Lett 7(9):2854–2858
45. Jain PK, El-Sayed MA (2008) J Phys Chem C 112:4954–4960
46. Tseng H-C (2010) Opt Expr 18(17):18360–18367
47. Stratton JA (2007) Electromagnetic theory. IEEE, New York
48. Park T-H, Nordlander P (2009) Chem Phys Lett 472:228–231
49. Korvink JG, Greiner A (2002) Semiconductors for Micro and Nanotechnology. Wiley, Weinheim
50. Jellison Jr. GE, Modine FA (1994) J Appl Phys 76(6):3758–3761
51. Nussenzveig HM (1992) Difraction effects in semiclassical scattering. Cambridge University Press, Cambridge
52. Van de Hulst HC (1957) Light scattering: by small particles. Dover, New York
53. Chu M-W (2009) Nano Lett 9(1):399–404
54. Nordlander P et al (2004) Nano Lett 4(5):899–903
55. Solis Jr. D et al (2012) Nano Lett 12:1349–1353
56. Noskov RE, Krasnok AE, Kivshar YS (2012) New J Phys 14(093005):1–10